Quantum and classical branching flow in space and time

Jakub Šťavina [*]

Department of Physics and Astronomy, The University of Manchester, Manchester M13 9PL, England, United Kingdom

Peter Bokes [†]

Faculty of Electrical Engineering and Information Technology, Institute of Nuclear and Physical Engineering,
Department of Physics, Slovak University of Technology in Bratislava, 812 19 Bratislava, Slovak Republic

Branching flow, a phenomenon known for steady wave propagation in two-dimensional weakly correlated random potential, is also present in the time-dependent Schrödinger equation for a single particle in one dimension, moving in a fluctuating random potential. We explore the two-dimensional parameter space of this model using numerical simulations and identify its classical regions, where just one classical parameter is sufficient for its specification, and its quantum region, where such a simplification is not possible. We also identify the region of the parameter space where known analytical results of a classical white noise model are relevant. Qualitative behavior of quantum and classical particle dynamics is discussed in terms of branching time scale and a new time scale related to a particle's kinetic energy.

I. INTRODUCTION

In 2001 Topinka *et al.* [1] discovered an interesting behavior of electrons entering a weakly perturbed two-dimensional (2D) degenerate electron gas through a narrow constriction. The electronic flow exhibited branching strands on a spatial scale larger than the correlation length of the perturbing potential. The phenomenon has been explained as a classical flow of particles in 2D weak short-ranged correlated random potential whose trajectories are repeatedly focused into caustics [1,2]. The flow has several universal statistical features [2,3] such as a simple scaling for the branching time t_b with its universal dependence on weak random potential amplitude strength $t_b \approx v_0^{-2/3}$. Behavior similar to branching flow has previously been known as an explanation for the appearance of large surface waves in oceans due to random topography of the ocean floor playing the role of weak random potential [4,5]. Motivated by the strongly anisotropic structure of the ocean floor caused by its geological history, the classical model describing the branching flow has been generalized for 2D anisotropic random potential with two different correlation lengths [6]. The importance of wave decoherence and smoothing of ray dynamics has been stressed for the appearance of branches with high intensity [7]. Recently, Patsyk *et al.* [8] observed branching flow of laser light in thin soap bubbles, which once again demonstrated the statistical characteristics of branching flow. Their experiment was so simple to understand and its results so beautiful that the effect found its way as one of the problems for the 34th International Young Physicists' Tournament in 2021 [9]. An overview and explanation of the branching flow phenomenon for a broader audience has recently been published in Ref. [10].

In our work we explore the signatures of branching flow phenomenon in the time-dependent Schrödinger equation for a single particle in one dimension (1D), moving in a fluctuating random potential. This is motivated by the similarity of the paraxial approximation for static 2D wave equation used for the description of branching flow [8] to the time-dependent Schrödinger equation. In our models the role of the static 2D correlated disorder is taken by a correlated fluctuating disordered potential $V(x, t)$. In contrast to the typically considered static disordered potential in two dimensions, the two variables x and t are quite distinct and the correlation of the potential energy is characterized by two independent parameters, the correlation length λ and the correlation time $\mathcal{T}$. This makes our problem mathematically similar to the anisotropic random potential considered by Degueldre *et al.* [6].

We study three levels of theory for the model: (1) a quantum particle in a fluctuating disordered potential, (2) a classical particle in a fluctuating disordered potential, and (3) a classical particle affected by a random force with white noise correlation function. The first two are studied numerically, and their mutual comparison leads to identification of a transition between quantum-mechanical and classical dynamics in an identically defined stochastic potential. This transition is also manifested through a reduction of the two-parametric system to a system with a single classical parameter. For the third case, which is a physically motivated approximation of the second one, we discuss available analytical results and compare them to numerical results for the first two cases. Based on this comparison we explore the limitations of the analytical formulas that can also be used for discussion of branching flow in a wider range of physical systems.

*[*]stavina.jakub@gmail.com

[†]peter.bokes@stuba.sk

II. QUANTUM PARTICLE IN FLUCTUATING DISORDERED POTENTIAL

We want to describe the dynamics of a quantum particle with mass m moving in one spatial dimension within a fluctuating disordered potential $V(x, t)$. The potential is a result of a certain stationary stochastic process with zero mean and prescribed correlation function,

$$\langle V(x' + x, t' + t)V(x', t')\rangle = V_0^2 s_x(x/\lambda)s_t(t/\mathcal{T}), \quad (1)$$

where V_0^2 gives the variance of the potential energy fluctuations, λ its correlation length in spatial dimension, and $\mathcal{T}$ its correlation time. The functions $s_x(z)$ and $s_t(z)$ are even, equal to 1 at $z = 0$, and decay quickly to zero. In our work we use Gaussians for both $s_x(z) = s_t(z) = \exp(-z^2/2)$. It has been claimed in the past that the typical behavior of the observed branching flow patterns is rather insensitive to the precise form of these functions [1,8].

In general, the averaging indicated by the brackets $\langle \cdots \rangle$ corresponds to ensemble average over many realizations of the potential. In our numerical simulations we consider a more restrictive ensemble of potentials, where Eq. (1) is satisfied by requiring each potential in the ensemble to fulfill $(LT)^{-1} \int_0^L dx' \int_0^T dt' V(x' + x, t' + t)V(x', t') = V_0^2 s_x(x/\lambda)s_t(t/\mathcal{T})$ for finite domains of integration L and T. This can be understood as averaging over potentials generated by a shift in space and time from a single realization only.

The correlation length implies a relevant spatial scale for the problem which we use as a unit of length, $x/\lambda \to x$. As a unit of time we choose a quantum time scale associated with a distance λ, $t/[(m\lambda^2)/\hbar] \to t$. Using these quantum units (q.u.), the Schrödinger equation for the particle is

$$i\frac{\partial\psi}{\partial t} = -\frac{1}{2}\frac{\partial^2\psi}{\partial x^2} + v_0\xi(x, t/\tau)\psi, \quad (2)$$

where $v_0 = (m\lambda^2/\hbar^2)V_0$, $\tau = \mathcal{T}/[(m\lambda^2)/\hbar]$ and $\langle\xi(x' + x, t' + t)\xi(x', t')\rangle = s(x)s(t)$. The use of quantum units results in two parameters v_0 and τ that define the fluctuating disordered potential. The meaning of v_0 is the ratio of the mean square fluctuation of the potential to the estimate of the ground state energy of a particle in a well of length λ, and the meaning of τ is the ratio of the fluctuating potential's correlation time to the estimate of the period of oscillation in time of the phase of a particle in the ground state of the well of length λ.

The expression $\tilde{v}_0 = v_0\tau^2$, when cast into SI units, gives $V_0\mathcal{T}^2/(m\lambda^2)$, i.e., an expression which is independent of Planck's constant. Hence, this combination remains finite in the classical limit and represents a single parameter of the system in the classical regime, which we confirm in the next section.

On the other hand, both τ as well as v_0 in SI units contain Planck's constant, and in the classical limit $\hbar \to 0$ we find $\tau \to 0$ and $v_0 \to \infty$. In view of their above interpretation using a quantum particle in a potential well, $v_0 \leqslant 1$ and at the same time $\tau \geqslant 1$ should imply nonclassical behavior. We note that $\tau \to \infty$ results in a static disorder, a situation studied in the theory of strong localization in 1D [11], and the limit $v_0 \to 0$ corresponds to a free quantum particle.

Formally, Eq. (2) is equivalent to the paraxial approximation of a stationary wave equation in 2D [8]. In the case of
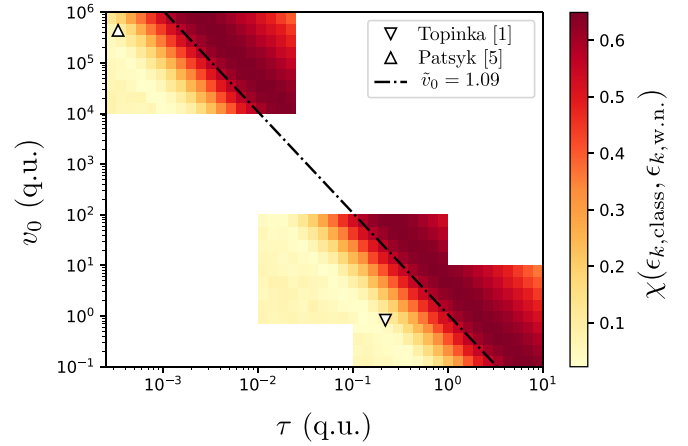

FIG. 1. The kinetic energy difference indicator for numerical solution of the classical model [Eq. (3)] and analytical results for the white noise models shown in color within the considered parameter space $\tau \times v_0$. Both models for different values of parameters are equivalent along the lines $\tilde{v}_0 = v_0\tau^2 = \text{const}$. In the left bottom part of the parameter space, left of the dashed line $\tilde{v}_0 = 1.09$ the results for numerical solution and the white noise model agree. Triangular symbols show the positions of parameters for systems experimentally studied by Topinka *et al.* [1] and Patsyk *et al.* [8].

light propagation in a thin soap film studied by Patsyk *et al.* [8], the correspondence is obtained using the following identifications: $v_0 = l_c^2 k_0^2 \bar{n}^2 u_0$ and $\tau = (k_0\bar{n}l_c)^{-1}$, where we use the notation from the original paper [8]: l_c is the correlation length of the 2D static disordered potential, k_0 the wave number of the light in the vacuum, and $u_0 = 0.5\sqrt{\langle n_{\text{eff}}^4\rangle/\bar{n}^4 - 1}$, with $\bar{n}$ and n_{eff} being the average and effective refractive index. Through this expression we find that, for example, for Fig. 3(a) in Ref. [8] the corresponding values of our parameters are $v_0 = 4.42 \times 10^5 \gg 1$ and $\tau = 3.36 \times 10^{-4} \ll 1$, so that we are safely in a classical regime. The classical parameter $\tilde{v}_0$ attains for this particular example the value $\tilde{v}_0 = v_0\tau^2 \approx 0.05$.

Similarly, we can relate the model defined by Eq. (2) to the branching flow observed in electronic flow through quantum point contact in 2D electron gas [1]. The paraxial approximation was not used in this work. Instead, the authors used a full 2D propagation for their simulations [12]. Nonetheless, to place their physical realization of branching flow into the parameter space of our model, we use the correspondence between the paraxial approximation to the time-independent Schrödinger equation in 2D and Eq. (2) that results in simple mapping between the parameters of both models: $v_0 = (m_e l_c^2/\hbar^2)V_0 \approx 0.83 \sim 1$ and $\tau = (k_F l_c)^{-1} \approx 0.22 \sim 1$, where k_F is the electron's Fermi wave vector, the correlation length of the 2D static disordered potential is l_c, and the square root fluctuation of the potential is V_0. These values of τ and v_0 indicate a quantum regime, while the classical parameter $\tilde{v}_0 \approx 0.04$ is similar to the case of light propagation in soap films [8]. The paraxial approximation for the stationary 2D wave equation is valid if $V_0 \ll \frac{\hbar^2 k_F^2}{2m}$, which, using the above correspondence, gives $\tilde{v}_0 \ll 1/2$. Similar criterion can be found for the laser beam propagation. Hence, a comparison
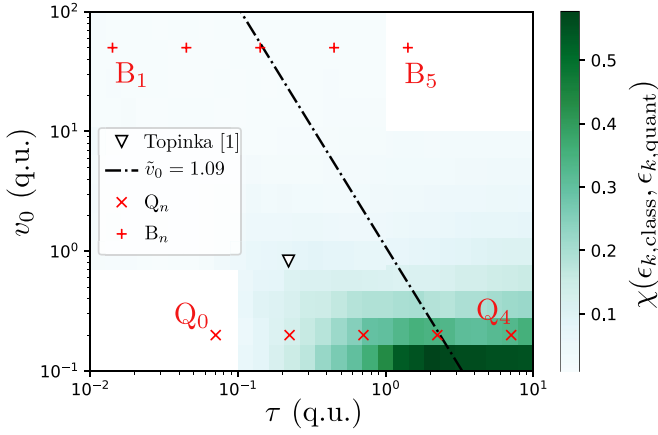
FIG. 2. The kinetic energy difference indicator for classical and quantum behavior. Points $B_n, n = 1, \ldots, 5$ and $Q_n, n = 0, \ldots, 4$ show the position of classical and quantum regimes, which we analyze as the fluctuating potential becomes slower (increasing τ). The triangular symbol gives the parameters of the system corresponding to that studied by Topinka *et al.* [1].
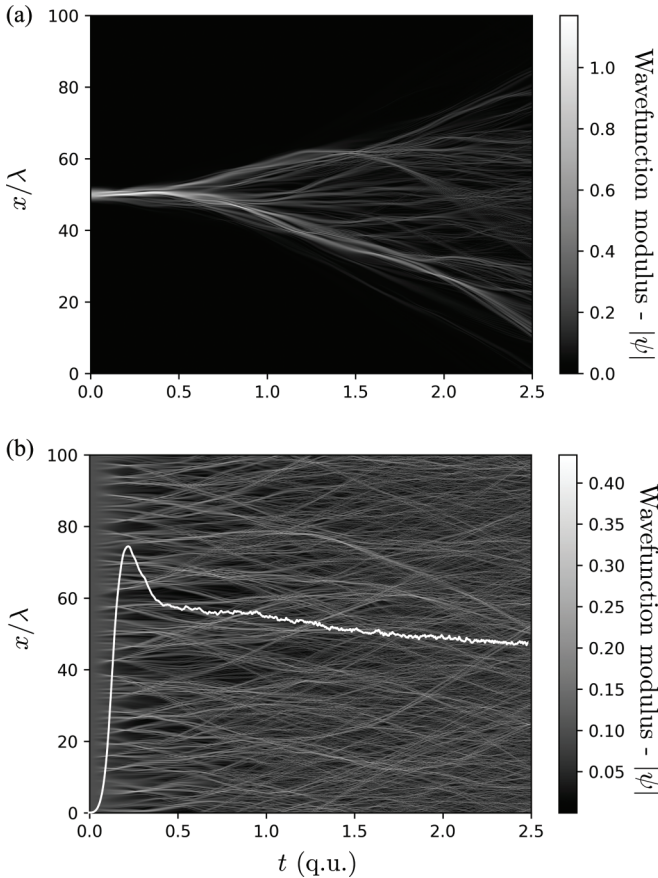

FIG. 3. Branching flow pattern of the propagated wave function amplitude for $v_0 = 50$ and $\tau \approx 0.05$ (B_2) when the initial condition is (a) a localized Gaussian wave packet and (b) a constant. Over the wave function amplitude in (b) we show the scintillation index having a pronounced maximum close to the branching time $t_b = 0.22$. Figures corresponding to other B_n/Q_n points can be found in Appendix B. The patterns corresponding to other B_n/Q_n points can be found in Figs. 9–20 in Appendix B.
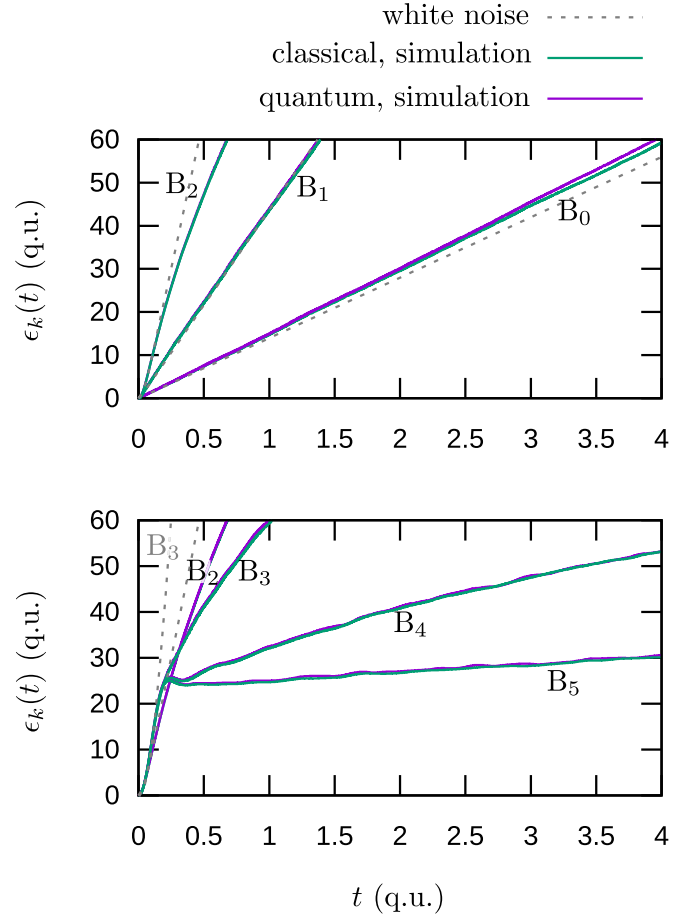

FIG. 4. Dependence of average kinetic energy on time for the series of "classical" points B_n in the parameter space. Up to $n = 2$ the white noise model is in agreement with both simulations; beyond $n = 2$ the behavior changes qualitatively.

between the results of our model and the two above physical systems can be made only in the regime $\tilde{v}_0 \ll 1$.

III. CLASSICAL AND WHITE NOISE MODELS

The classical equation of motion corresponding to the dynamics of quantum particles from the previous section is

$$\ddot{x} = -v_0 \frac{\partial}{\partial x} \xi(x, t/\tau). \tag{3}$$

Here, however, one may reduce the two parameters v_0 and τ to one by rescaling the units of time once again according to $t/\tau \to t$, with the result of having a single classical parameter $\tilde{v}_0 = v_0 \tau^2$ identified in Sec. II based on dimensional analysis. This parameter sets the strength of the fluctuating force $f(x, t) = -\tilde{v}_0 \frac{\partial}{\partial x} \xi(x, t)$ on the right-hand side of a rescaled version of Eq. (3).

To obtain a couple of analytical results we use an *ad hoc* approximation to the fluctuating force $f(x, t)$ in the form of a spatially uncorrelated random force $f(t)$ with $\langle f(t) \rangle = 0$ and $\langle f(t) f(t') \rangle = \tilde{v}_0^2 s(t - t')$. In other words, we assume that this force's time correlation function inherits the correlation time τ ($\tau = 1$ in the rescaled units) of the original potential $V(x, t)$ from Eq. (1). Within this approximation it is possible to show
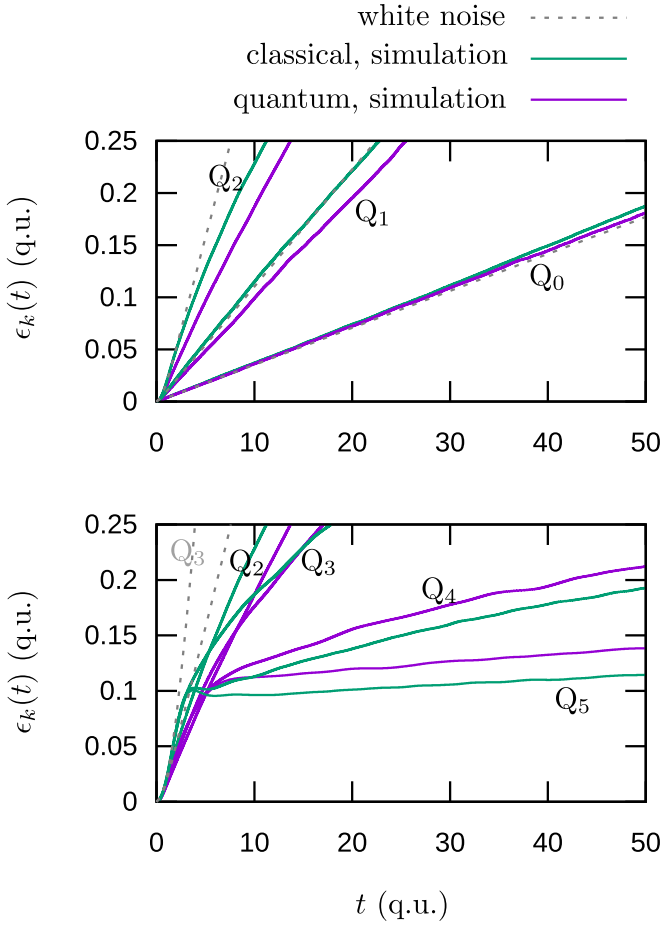
FIG. 5. Dependence of average kinetic energy on time for the series of quantum points Q_n in the parameter space. Similarly to the B_n points, the behavior changes qualitatively for $n = 2$, but now the classical and quantum simulations do not agree quantitatively.
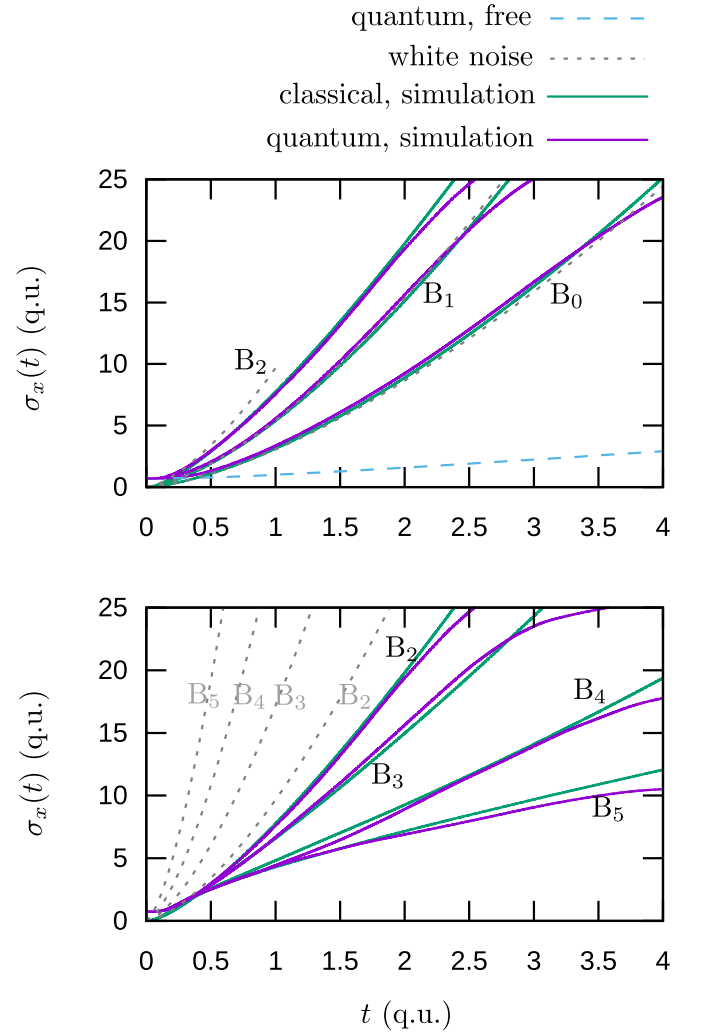

FIG. 6. Dependence of the root-mean-square displacement on time in the classical region of the parameter space. Close to $n = 2$ the numerical solutions lead to qualitatively different results from the white noise model.

that the average kinetic energy of a particle is given by the expression

$$\langle e_k(t) \rangle = e_k(0) + \tilde{v}_0^2 \sqrt{\pi} \int_0^{t/\sqrt{2}} \text{erf}(z) dz. \tag{4}$$

An even simpler model for the fluctuating force, used by several studies in the past [2,6], is the white noise model of the fluctuating force,

$$f_{\text{w.n.}}(t) = \gamma \Gamma(t), \quad \langle \Gamma(t) \Gamma(t') \rangle = \delta(t - t'), \tag{5}$$

for which the average kinetic energy of a particle is given by a simple expression,

$$\langle e_k(t) \rangle = e_k(0) + \gamma^2 t. \tag{6}$$

Identical linear growth in time is also obtained from the long-time behavior of the average kinetic energy from Eq. (4) for $\gamma^2 = \tilde{v}_0^2 \sqrt{\pi/2}$. In other words, the white noise model is an approximation to the random force model valid for times $t \gg \tau = 1$. Hence, its predictions need to be limited to the time scales that are larger than the fluctuating potential's correlation time at best.

The second quantity of interest for which an analytical result for the white noise model is available [6] is the average square of the particle's displacement $\sigma_x^2(t) = \langle [x(t) - x(0)]^2 \rangle$,

$$\sigma_x^2(t) = \dot{x}(0)^2 t^2 + \tfrac{2}{3} \gamma^2 t^3. \tag{7}$$

This relation is obtained by a direct integration of the expression $\frac{d}{dt} \langle [x(t)]^2 \rangle = 2 \langle x(t) \dot{x}(t) \rangle$, where $x(t)$ and $\dot{x}(t)$ are expressed as formal time integrals of the stochastic equation of motion $\ddot{x} = f_{\text{w.n.}}(t)$.

From the two analytical results [Eqs. (6) and (7)] we can obtain estimates of two different time scales encountered in the dynamics of particles in fluctuating disordered potential. In their calculation we will assume that the initial average kinetic energy is negligible compared to the kinetic energy attained by the particle in the course of its motion.

The branching time t_b is defined as the time for which the average displacement Eq. (7) is equal to the correlation length
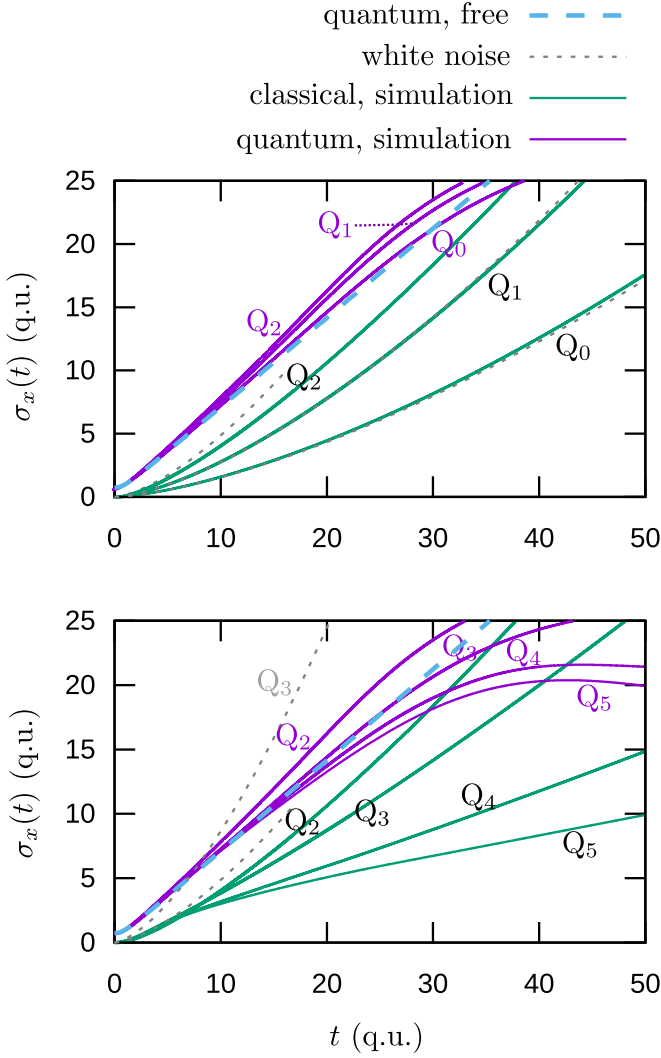
FIG. 7. Dependence of the root-mean-square displacement on time in the quantum region of the parameter space. The behavior of the quantum simulation is dominated by the quantum dispersion of a free particle.

λ ($\lambda = 1$ in our present units) of the disordered potential,

$$t_b = \left(\frac{3}{2\gamma^2}\right)^{1/3} = \left(\frac{9}{2\pi}\right)^{1/6} \tilde{v}_0^{-2/3}. \tag{8}$$

As noted earlier, the validity of the white noise model is limited at best to time scales $t_b \gg \tau = 1$, which results in the requirement $\tilde{v}_0 \ll [9/(2\pi)]^{1/4} \approx 1.09$.

Since the kinetic energy in the random force model increases with time, we also define time t_e as the instance when the average kinetic energy is equal to the square root dispersion of the potential energy fluctuations,

$$t_e = \frac{\tilde{v}_0}{\gamma^2} = \frac{1}{\sqrt{\pi/2}\tilde{v}_0}. \tag{9}$$

If this estimate could also be used within the fluctuating potential model, then it would indicate that beyond this time scale the particle will propagate over long distances and it would not be bound within a local minimum of the potential.
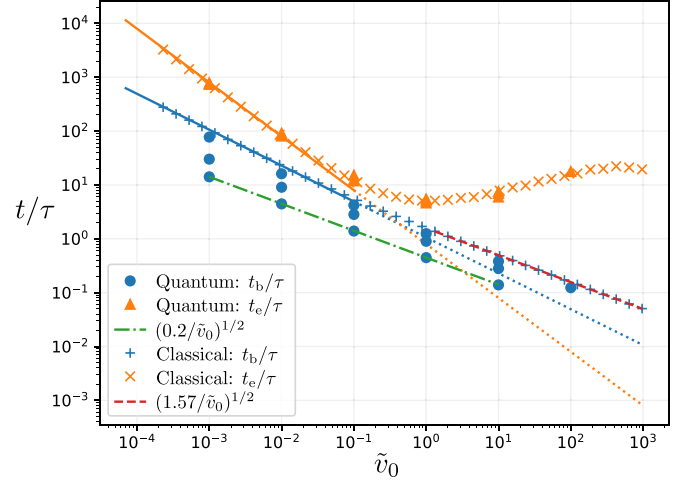

FIG. 8. For $\tilde{v}_0 \ll 1$ the white noise model prediction for both time scales $t_b \approx \tilde{v}_0^\beta$, $\beta = -2/3$ and $t_e \approx \tilde{v}_0^\epsilon$, $\epsilon = -1$ (full lines) agrees with the classical numerical simulations. At the edge of its validity, $\tilde{v}_0 \approx 1$, the two time scales approach each other, but eventually separate. The branching time follows a new power law characterized by exponents $\beta = -1/2$ and the energy time scale attains a well-defined minimum. When quantum effects are important the branching time is not a universal function of $\tilde{v}_0$; the vertically stacked circles correspond to identical $\tilde{v}_0$ and differ in v_0. In our simulations t_b in the quantum regime is dominated by wave packet quantum dispersion, which is also characterized by the exponent $\beta = -1/2$. In contrast, the kinetic energy time scale t_e, obtained from the plane wave initial condition, keeps following the classical behavior.

The usefulness of these formulas rests on the validity of the white noise model for the fluctuating random potential. To explore this we have performed numerical simulations for both the classical and the quantum system with fluctuating disordered potential that are discussed in the next section.

IV. NUMERICAL SIMULATIONS

In our numerical simulations we used quantum units introduced in Sec. II for quantum as well as the classical dynamics. The analytical results from the previous section using the quantum units are

$$\langle e_k(t)\rangle = e_k(0) + \sqrt{\frac{\pi}{2}}v_0^2\tau t \tag{10}$$

$$\sigma_x^2(t) = \dot{x}(0)^2 t^2 + \frac{\sqrt{2\pi}}{3}v_0^2\tau t^3 \tag{11}$$

$$t_b = \left(\frac{9}{2\pi}\right)^{1/6} v_0^{-2/3}\tau^{-1/3} \tag{12}$$

$$t_e = \frac{1}{\sqrt{\pi/2}v_0\tau}. \tag{13}$$

Realizations of the functional form of the fluctuating disordered potential $\xi(x,t)$ in Eq. (2) are generated using uniform random distribution for the phases of its Fourier series $\mathcal{F}[\xi](k_n, \omega_m)$ in the domain $(x,t) \in (0, L) \times (0, T)$. The magnitude of the Fourier coefficient is determined by the Fourier coefficient $\mathcal{F}[s](k_n)$ of the correlation
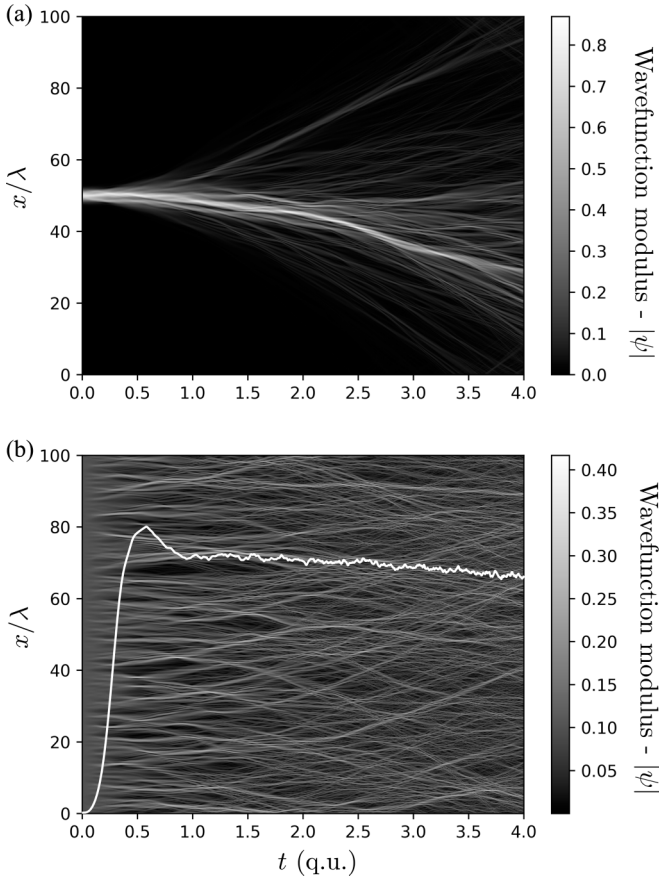
FIG. 9. B_0; $v_0 = 50$ and $\tau = 4.47 \times 10^{-3}$.
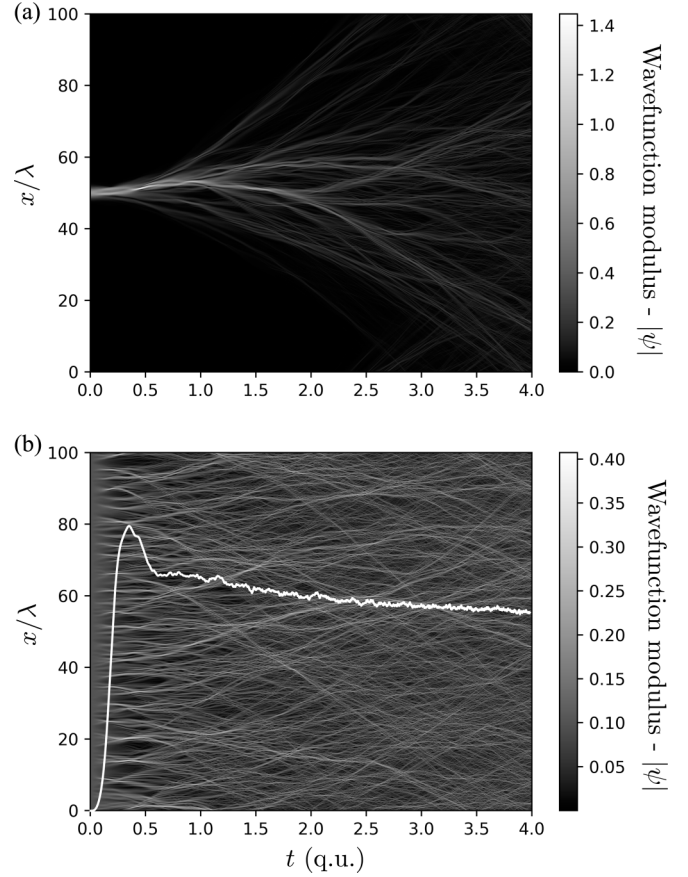
FIG. 10. B_1; $v_0 = 50$ and $\tau = 1.41 \times 10^{-2}$.

functional form $s(z)$ [Eq. (1)] by the expression $|\mathcal{F}[\xi](k_n, \omega_m)| = \sqrt{|\mathcal{F}[s](k_n)||\mathcal{F}[s](\omega_m)|}$. In this way the ensemble of generated potentials fulfills correlation function Eq. (1) by construction. (See Appendix A for more details.)

Samples of potentials have been generated on a spatial domain $x \in (0, 100)$ with typically $N = 8000$ samples and on a time domain $t \in (0, 5t_b)$ with typically $M = 30\,000$ samples for the purpose of parameter space scanning presented in Figs. 1 and 2. For longer runs (larger value of T) the time step Δt was chosen so as to keep the ratio $\Delta t/(\Delta x^2) = 1$, where $\Delta x = L/N$, which resulted in satisfactory stability of numerical integration of both classical as well as quantum equations of motion.

The classical simulations were performed using a second-order Störmer–Verlet integrator for a set of 4000 initial positions uniformly distributed over the whole spatial domain. The initial velocity was set to zero. From a sample of 104 random fluctuating potentials, each with all 4000 initial positions, we calculated the time evolution of the average kinetic energy $\epsilon_{k,\text{class}}(t) = \langle \frac{1}{2}\dot{x}(t)^2 \rangle$, and the time evolution of the root-mean-square displacement of the particle's coordinate $\sigma_{x,\text{class}}(t) = \sqrt{\langle [x(t) - x(0)]2 \rangle}$.

The quantum simulations were performed using the split-step Fourier method, which utilizes the Suzuki-Trotter formula for the time evolution operator. The potential energy term of the Hamiltonian was propagated in the real space and the kinetic energy term was propagated in the Fourier space. We have used two kinds of initial conditions: a single

Gaussian wave packet with unit width localized in the center of the simulation domain ($x = L/2$) for the calculation of the mean square displacement of a particle's coordinate and a constant amplitude ("plane wave") over the whole simulation domain for the calculation of the average kinetic energy and the scintillation index (see below). The initial kinetic energy of the plane wave state is negligible, whereas the localized initial condition in the form of a Gaussian of unit width has the initial kinetic energy $\epsilon_{k,\text{quant}}(0) = 1/4$. The root-mean-square displacement for the Gaussian initial condition is $\sigma_{x,\text{quant}}(0) = 1/\sqrt{2}$. Similarly to the classical simulations, for 104 samples of random potentials, we calculated the average kinetic energy $\epsilon_{k,\text{quant}}(t) = -\langle \int \psi^*(x, t) \frac{1}{2} \frac{\partial^2}{\partial x^2} \psi(x, t) dx \rangle$ for the plane wave initial conditions and the root-mean-square displacement of the particle's coordinate $\sigma^2_{x,\text{quant}}(t) = \langle \int |\psi(x, t)|^2 (x - L/2)^2 dx \rangle$ for the initial condition localized at $x = L/2$, in the center of the simulation box. Due to the finite simulation domain the displacement calculation does not lead to useful results when the amplitude of the wave function is noticeable at the box boundaries $x = 0$ or $x = L$. Hence, this quantity will be taken into account only for a limited time of simulation. In contrast, the average kinetic energy is insensitive to the boundary condition due to the fluctuating nature of the potential. This is also the reason why plane wave initial condition is suitable for its calculation.

We have performed the above described calculations for a wider region of models' parameter space, which is shown in
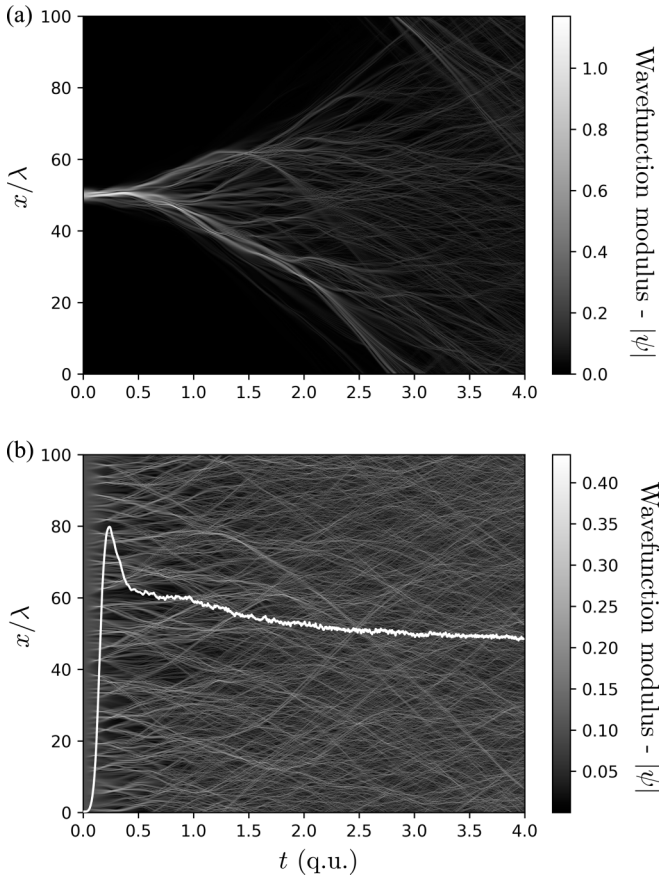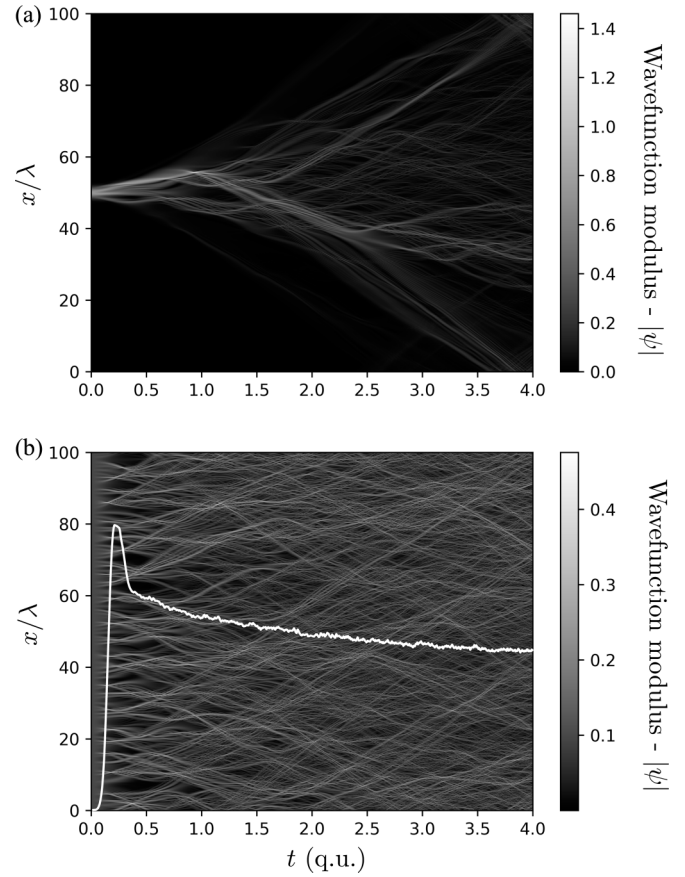
FIG. 11. B_2; $v_0 = 50$ and $\tau = 4.47 \times 10^{-2}$.

FIG. 12. B_3; $v_0 = 50$ and $\tau = 1.41 \times 10^{-1}$.

Fig. 1. To quantify differences between the time dependence of the average kinetic energy calculated for two different models we use an indicator χ attributed to two functions $a(t)$, $b(t)$ by the formula $\chi(a, b) = \sqrt{\sum_{i=1}^{M} [1 - a(t_i)/b(t_i)]^2/M}$, where $\{t_i\}_{i=1}^{M}$ is the used time discretization. From Fig. 1 we can clearly see that approximating the fluctuating random potential by the white noise model does indeed describe the behavior well if the condition $\tilde{v}_0 \ll 1$ is fulfilled. The figure also demonstrates that the classical models depend only on the classical parameter $\tilde{v}_0 = v_0 \tau^2$ and not on the two parameters v_0 and τ separately. In contrast, comparison of the numerical simulations of the classical and the quantum particle in Fig. 2 shows that the quantum model depends on two separate parameters in the nonclassical region of the parameter space, $\tau > 1$ and $v_0 < 1$. This also confirms the criteria for quantum behavior stated in Sec. II.

The wave function modulus $|\psi(x, t)|$ for the specific quantum simulation with $\tau \approx 0.05$ and $v_0 = 50$ ($\tilde{v}_0 = 0.125$) is shown in Fig. 3. Both localized and plane wave initial conditions result in typical branching flow patterns for this value of parameters. The scintillation index, $S(t) = \langle(\int |\psi(x, t)|^4 dx)/\langle\int |\psi(x, t)|^2 dx)^2 - 1$ [8], is shown by the white curve on top of the amplitude for plane wave initial condition and it exhibits a maximum close to the branching time t_b. We note that in the quantum regime this feature of the scintillation index disappears, as demonstrated in Figs. 15–20 in Appendix B.

In Figs. 4–7 we quantify the dynamics of classical and quantum simulations for two considered sequences of points B_n ($v_0 = 50$) and Q_n ($v_0 = 0.2$) from the parameter space. Both sequences of points correspond to an identical sequence of the parameter $\tilde{v}_0 = 10^{n-3}$, $n = 0, \ldots, 5$ and differ only in the importance of quantum effects: B_n are well in the classical regime, whereas Q_n increase their quantum character along the sequence (see also Fig. 2). This choice is motivated by the fact that for the two experimental studies [1,8] discussed at the end of Sec. II, the branching flow pattern has been observed for $\tilde{v}_0 \approx 0.05$, i.e., between the points with $n = 1$ and $n = 2$.

First we discuss the behavior of the average kinetic energy shown in Figs. 4 and 5. Whereas for B_0 and B_1 the average kinetic energy agrees well with the prediction of the white noise model within the studied time interval, for points $B_n, n \geqslant 2$ ($\tilde{v}_0 \geqslant 0.1$) it attains much lower values, exhibits concave character, and is qualitatively different from the white noise model: by increasing $\tilde{v}_0$, the rate of growth of the kinetic energy decreases. Still, for a given $\tilde{v}_0$ the kinetic energy steadily grows with time, and at some point it reaches the characteristic magnitude of potential fluctuation v_0 so that the characteristic time t_e can be unambiguously determined from the equation $\epsilon_k(t_e) = v_0$. For all the B_n points the quantum and the classical simulations give very similar results, since here $v_0 \gg 1$, i.e., one of the two possible conditions discussed in Sec. II for classical behavior is fulfilled. The above described qualitative change in the behavior of the average kinetic energy exhibits the model in the quantum regime as well, as demonstrated in
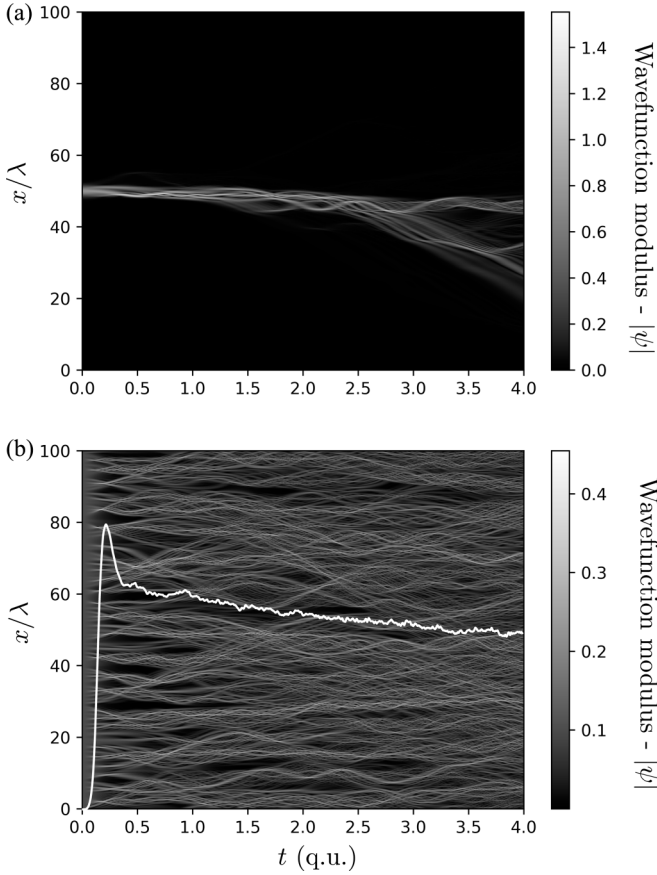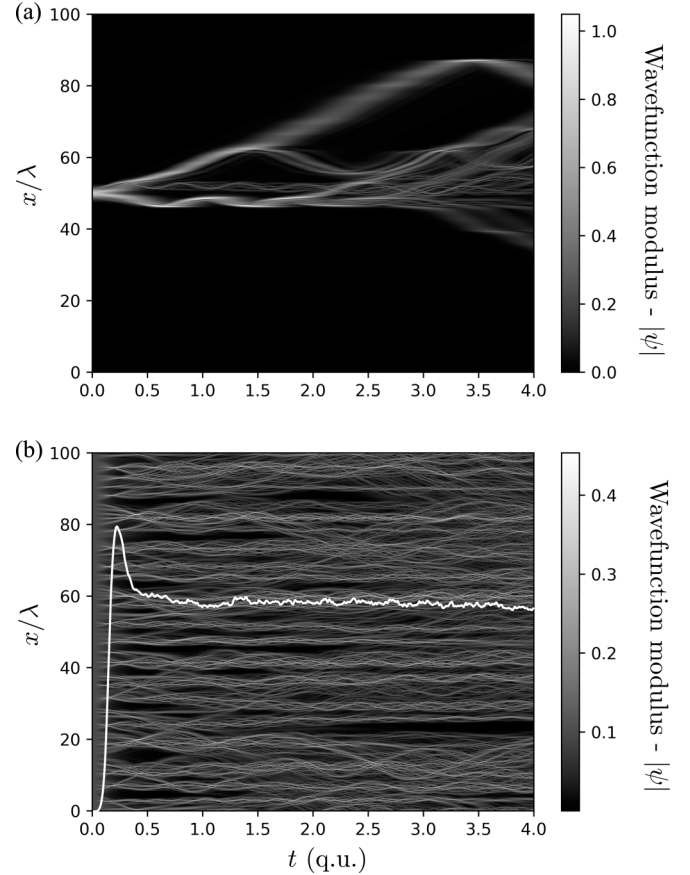
FIG. 13. B_4; $v_0 = 50$ and $\tau = 4.47 \times 10^{-1}$.

FIG. 14. B_5; $v_0 = 50$ and $\tau = 1.41 \times 10^0$.

Fig. 5, except that now the classical and quantum simulations are not in quantitative agreement (see also Fig. 2).

Similarly, the root-mean-square displacements depart from the white noise model as we move towards larger $\tilde{v}_0$ in the parameter space. In Fig. 6, for B_n, $n = 0, 1, 2$ we see a good agreement between the white noise model and both classical and quantum simulations, and as of $n = 3$ the behavior between the white noise model and the two simulations is qualitatively different. For Q_n points (Fig. 7) the root-mean-square displacement obtained from the quantum simulations is affected by the uncertainty of the initial state—all the curves are very close to the free wave packet dispersion $\sigma_{x,\text{quant}}^{\text{free}}(t) = \sqrt{(1 + t^2)/2}$, which is the dominant mechanism for its growth. For larger times the curves for the quantum simulations bend downwards due to periodic boundary conditions. Nonetheless, it is clear that for this portion of the parameter space the increase in dispersion is not due to the fluctuating random potential but to the inherent uncertainty of particle velocity set in its initial condition.

From the above described simulations we obtained the numerically determined times $t_{b,\text{class}}$, $t_{b,\text{quant}}$ and $t_{e,\text{class}}$, $t_{e,\text{quant}}$ directly from their definitions $\sigma_x^2(t_b) = 1$ and $\epsilon_k(t_e) = v_0$, respectively. In the region of the phase space where the classical model is valid we expect that these time scales, when expressed in units of τ, depend solely on a single parameter $\tilde{v}_0 = v_0 \tau^2$. The resulting dependencies are shown in Fig. 8. For $\tilde{v}_0 < 1$ the white noise model prediction is in agreement with the numerical simulation with fluctuating random potential.

The branching time t_b/τ keeps decreasing even for $\tilde{v}_0 > 1$ but with a different scaling exponent $t_b/\tau \approx \tilde{v}_0^{\beta}$, $\beta = -1/2$. This can be understood as a short transient process in an essentially time-independent random potential ($t \ll \tau$, i.e., particles' energy is nearly conserved) when the initially homogeneously distributed positions of classical particles with zero kinetic energy start to move towards the local minima of potential energy. The time to traverse a single correlation length $\lambda = 1$ can then be estimated from a classical formula obtained from Eq. (3) and the energy conservation,

$$\frac{t_b}{\tau} = \int_{x_0}^{x_0+1} \frac{dx}{\sqrt{2\tilde{v}_0[\xi(x_0,0) - \xi(x,0)]}} \approx \tilde{v}_0^{-1/2}, \quad (14)$$

where x_0 is an initial position of a particle (in units of λ).

The kinetic energy timescale t_e attains a minimum value for $\tilde{v}_0 \approx 1.0$, and for larger strengths of the potential grows again, but the growth is not monotonic. We did not explore its behavior further, as our interest was only in parameter values a few orders of magnitude around the experimentally observed systems with branching flow, and at the same time, the numerical simulations for higher values of $\tilde{v}_0$ were becoming more demanding.

The time scales need not depend on a single parameter $\tilde{v}_0 = v_0 \tau^2$ for points in parameter space where quantum effects are important. We have seen this behavior already in Fig. 2, and it can also be manifestly demonstrated in the limit of a free quantum particle $v_0 \to 0$, $t_{b,\text{quant}}^{\text{free}}/\tau = 1/\tau =$
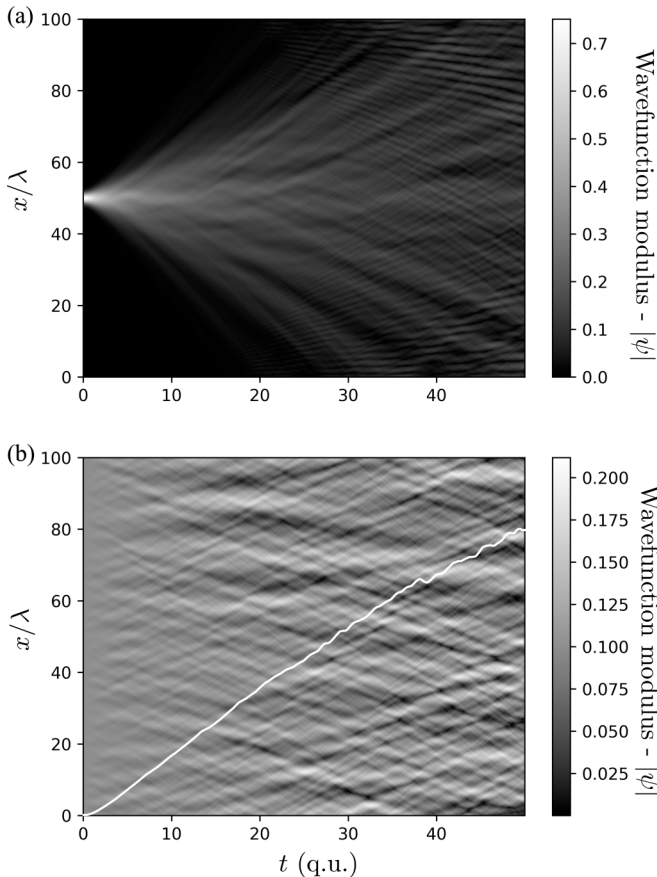
FIG. 15. Q_0; $v_0 = 0.2$ and $\tau = 7.07 \times 10^{-2}$.
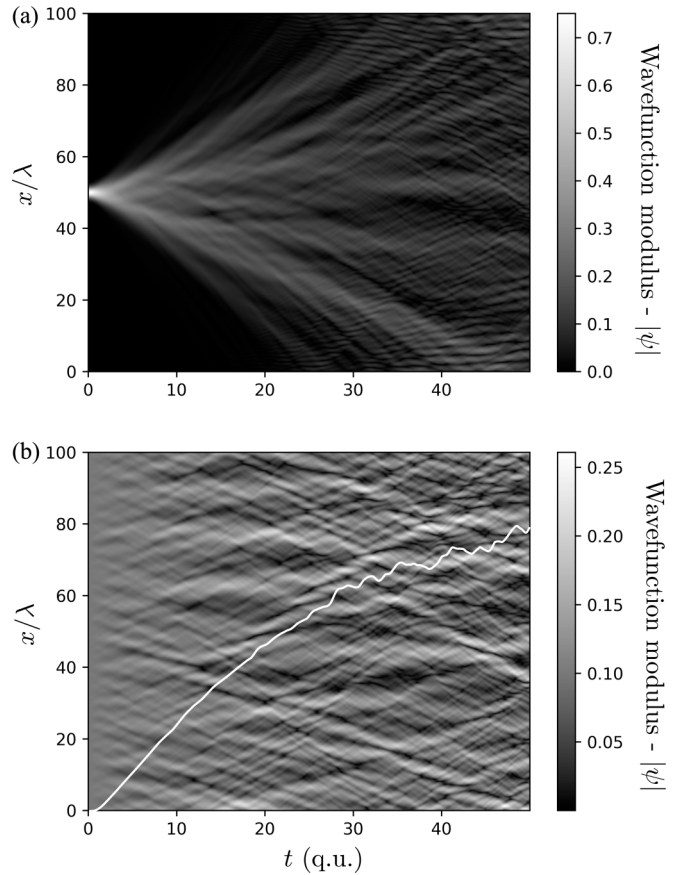
FIG. 16. Q_1; $v_0 = 0.2$ and $\tau = 2.24 \times 10^{-1}$.

$\sqrt{v_0/\tilde{v}_0}$. The dependence of the branching time for the Q_n points in Fig. 8 is clearly of this form, with exponent $\beta = -1/2$ and a constant shift in a logarithmic scale that depends on v_0. Obviously, for a different choice of the initial Gaussian wave packet, the dominance of the quantum wave packet dispersion appears for different regions of the parameter space. In contrast, $t_{e,\text{quant}}$ stays close to the classical results even for the points in parameter space where quantum effect are relevant. In this case we are following the evolution of a plane wave with practically zero initial kinetic energy. In the case of initial condition in the form of a Gaussian, the initial kinetic energy is nonzero [$\epsilon_{k,\text{quant}}(0) = 1/4$ in our simulations]. Specifically, for Q_n points this is above $v_0 = 0.2$, so this time scale would be meaningless.

V. CONCLUSIONS

In our work we have explored the phenomenon of branching flow for quantum and classical particles moving in a short-ranged randomly fluctuating potential in 1D and the validity of the classical white noise model for its description. For this purpose we have introduced an energy time scale t_e that complements the branching time t_b. In the classical regime the behavior of these two time scales can be well described within a white noise model for the random force as long as its strength parameter $\tilde{v}_0 \leqslant 0.1$. For $\tilde{v}_0 > 1.0$ the branching time is described by a different scaling exponent for which we have provided a simple physical explanation in terms of a

short time dynamics in a vicinity of a local minimum in the random potential. The energy time scale t_e attains a minimum for $\tilde{v}_0 \approx 1$ and grows nonmonotonically beyond this value for $\tilde{v}_0 > 1.0$. Interestingly, for the values of $\tilde{v}_0 \approx 0.01$–0.1, where branching flow has been experimentally observed in the past, these two time scales are closest to each other. This can be understood by ruling out the other possibilities as follows: for $\tilde{v}_0 > 1.0$ the branching pattern disappears due to stronger localization of the particles/waves, and for $\tilde{v}_0 \ll 1.0$ the t_e is too large so that it takes too much time to develop a widely branched pattern. Hence, for experimental observation it is preferable to have as small t_e as possible, as long as the localization does not take over.

We have discussed that the importance of quantum effects is accompanied by a loss of simple dependence of the system's behavior on a single parameter $\tilde{v}_0 = v_0 \tau^2$; instead, both the random potential root-mean-square amplitude v_0 and its correlation time τ have to be considered as independent parameters. The quantum effects are important if two conditions $v_0 < 1$ and $\tau > 1$ are fulfilled at once, which we have expected based on dimensional arguments and confirmed by extensive numerical simulations.
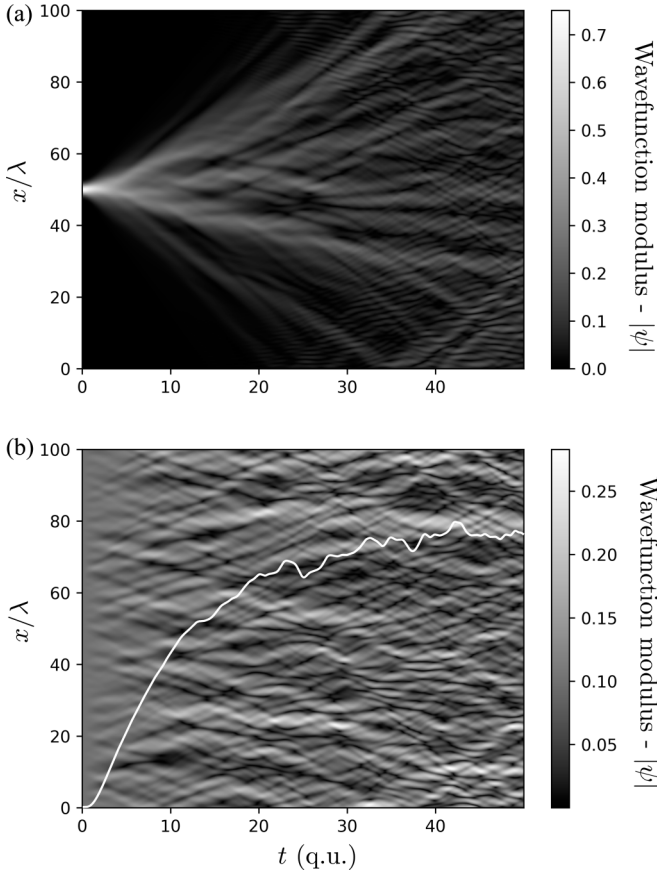
FIG. 17. Q_2; $v_0 = 0.2$ and $\tau = 7.07 \times 10^{-1}$.
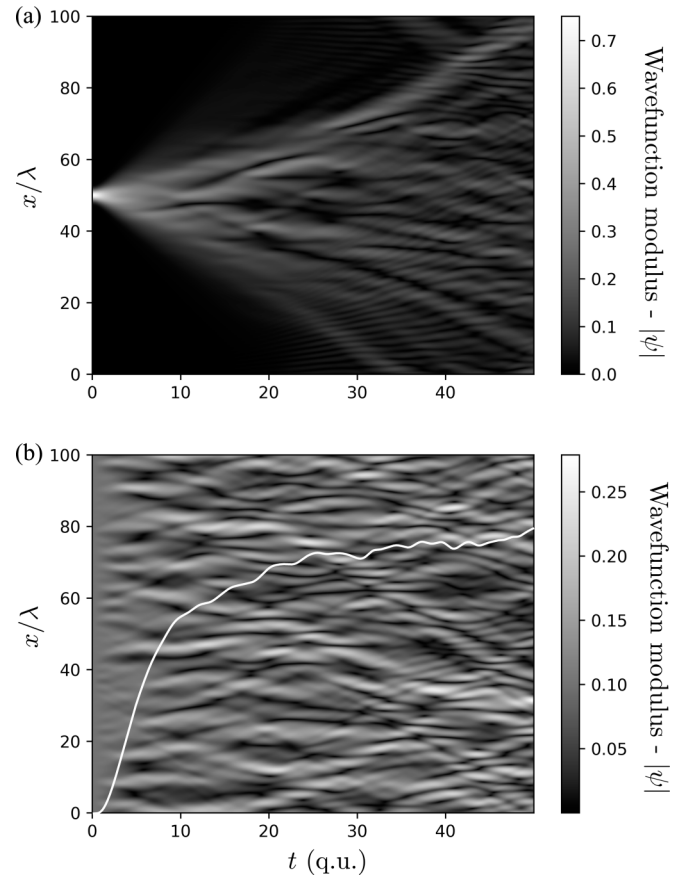
FIG. 18. Q_3; $v_0 = 0.2$ and $\tau = 2.24 \times 10^0$.

APPENDIX A: NUMERICAL IMPLEMENTATION

A study of a quantum particle in a fluctuating disordered potential requires solving Eq. (2) numerically. For this, we apply the split-step Fourier method, which utilizes Suzuki-Trotter expansion of the time evolution operator $\hat{U}(\delta t) = \exp[-i(\hat{T} + \hat{V})\delta t]$ that arises in the formal solution $\psi(x, t + \delta t) = \hat{U}(\delta t)\psi(x, t)$ to Eq. (2), as

$$\psi(x, t + \delta t) = (e^{-i\hat{V}\frac{\delta t}{2}} e^{-i\hat{T}\delta t} e^{-i\hat{V}\frac{\delta t}{2}})\psi(x, t) + \mathcal{O}(\delta t^3),$$

(A1)

where $\hat{T} = \frac{1}{2}p^2$ and $\hat{V} = v_0 \xi(x, t/\tau)$ are the kinetic and potential energy operators in momentum and position representations, respectively. This decomposition allows us to apply each part of the $\hat{U}(\delta t)$ operator to $\psi(x, t)$ as a multiplication in their respective representations. The transition between the position and momentum representations via Fourier transform is

$$\psi(x, t + \delta t) = e^{-iV(x,t)\frac{\delta t}{2}} \mathcal{F}^{-1}\{e^{-\frac{i}{2}p^2\delta t}$$

$$\times \mathcal{F}[e^{-iV(x,t)\frac{\delta t}{2}} \psi(x, t)]\} + \mathcal{O}(\delta t^3). \quad (A2)$$

In the numerical implementation the Fourier transform is approximated by a discrete Fourier transform (DFT). The DFT forces a periodic boundary on the space domain of a given length L, which means that the random potential $\xi(x, t)$ is also numerically seen as periodic with that given period L. This is used in its construction using the DFT. The spatial part

of the correlation function $s(x)$ is then specified on a finite interval $[-L/2, L/2]$ by the Gaussian centered at $x = 0$ with an additional condition $s(x) = s(x + L)$ for all x.

As discussed in Sec. II, we consider a restricted ensemble of random potentials $\xi(x, t)$ that consists of real-valued functions satisfying the condition

$$s(x)s(t) = \frac{1}{LT} \int_0^L dx' \int_0^T dt' \, \xi(x', t')\xi(x' + x, t' + t).$$

(A3)

In discrete form, over the domain $x_n = \{\frac{nL}{N}\}_{n=1}^N$ and $t_m = \{\frac{mT}{M}\}_{m=1}^M$, Eq. (A3) becomes $s(x_\alpha)s(t_\beta) = \frac{1}{NM} \sum_n \sum_m \xi(x_n, t_m)\xi(x_n + x_\alpha, t_m + t_\beta)$, which can be shown to equal

$$s(x_\alpha)s(t_\beta) = \frac{1}{(NM)^2} \sum_{n=1}^N \sum_{m=1}^M |\mathcal{F}[\xi](k_n, \omega_m)|^2 e^{i(k_n x_\alpha + \omega_m t_\beta)},$$

(A4)

with $\mathcal{F}[\xi](k_n, \omega_m)$ now signifying the DFT of ξ. By comparing Eq. (A4) to the inverse discrete Fourier transform of $s(x_\alpha)s(t_\beta)$, we conclude that the equality

$$\mathcal{F}[\xi](k_n, \omega_m) = \sqrt{NM \, \mathcal{F}[s(\cdot)s(\cdot)](k_n, \omega_m)} e^{i\phi(k_n, \omega_m)} \quad (A5)$$

must hold. Hence, to fulfill constraint (A4), the modulus of the DFT of $\xi(x, t)$ is fixed, while the phases $\phi(k_n, \omega_m)$ can
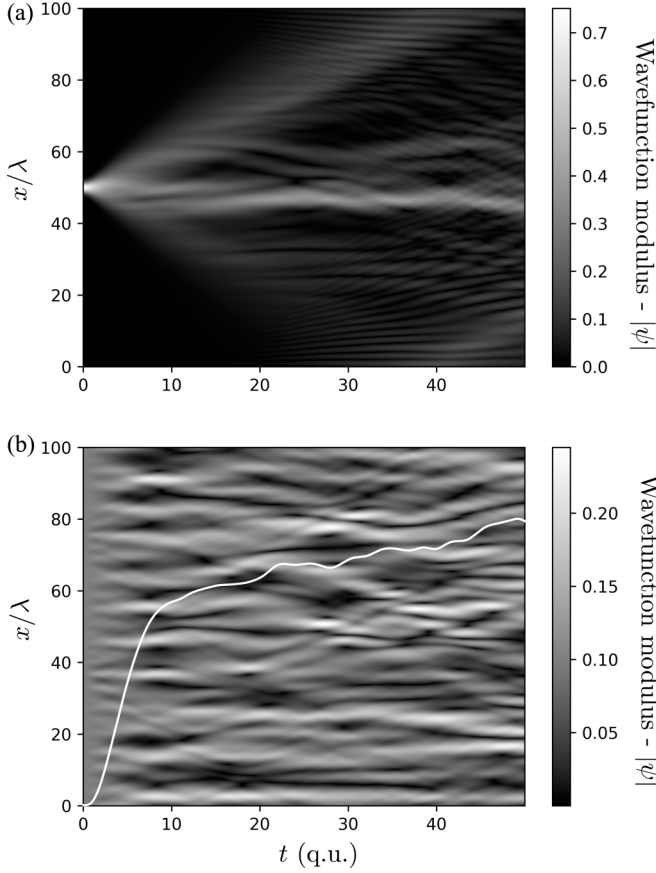
FIG. 19. Q_4; $v_0 = 0.2$ and $\tau = 7.07 \times 10^0$.
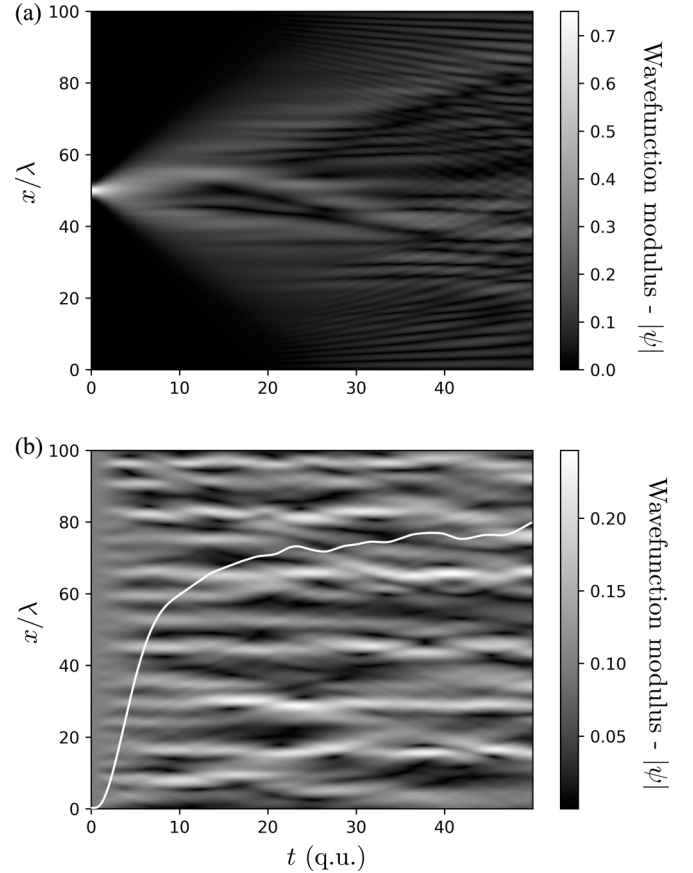
FIG. 20. Q_5; $v_0 = 0.2$ and $\tau = 2.24 \times 10^1$.

be chosen at random under the additional constraint that the resulting $\xi(x, t)$ is real-valued. This latter constraint reads $\mathcal{F}[\xi](k_n, \omega_m) = (\mathcal{F}[\xi])^*(2\pi N/L - k_n, 2\pi M/T - \omega_m)$ for the DFT of $\xi(x, t)$. It follows that for the phases $\phi(k_n, \omega_m)$ we demand

$$\phi(k_n, \omega_m) = -\phi\left(\frac{2\pi N}{L} - k_n, \frac{2\pi M}{T} - \omega_m\right). \quad \text{(A6)}$$

From the numerical solutions we obtain approximations for the time evolution of several observables. These are calculated from the $N \times M$ array of complex numbers $\psi(x_n, t_m)$ that approximates the wave function. The kinetic energy e_k, given by $\int dx \, \psi^*(-\frac{1}{2}\frac{\partial^2}{\partial x^2})\psi$, is in discretized form approximated as

$$e_k(t) \approx \delta x \sum_{n=1}^{N} \psi^*(x_n, t)\mathcal{F}^{-1}\left[\frac{p(\cdot)^2}{2}\mathcal{F}[\psi]\right](x_n, t), \quad \text{(A7)}$$

where we employ the discrete Fourier transform in a manner similar to the one used in Eq. (A2). The mean square displacement σ_x^2 is given by $\int dx \, \psi^*(x - L/2)^2\psi$ and hence is calculated as

$$\sigma_x^2(t) \approx \delta x \sum_{n=1}^{N} \left(x_n - \frac{L}{2}\right)^2 |\psi(x_n, t)|^2. \quad \text{(A8)}$$

A quantity studied in connection with the branching flow is the scintillation index defined as $S = \langle(\psi^*\psi)^2\rangle/\langle\psi^*\psi\rangle^2 - 1$ [8]. From our simulations its value is obtained as

$$S(t) \approx \frac{\sum_{n=1}^{N} |\psi(x_n, t)|^4}{\left(\sum_{n=1}^{N} |\psi(x_n, t)|^2\right)^2} - 1. \quad \text{(A9)}$$

We note that these quantities are further averaged over an ensemble of random potentials, differing by random phases ϕ. For the classical simulation, the relevant studied characteristics are obtained directly from the trajectories $x(t)$. The latter are obtained numerically using the Störme-Verlet method for Eq. (3).

APPENDIX B: BRANCHING FLOW PATTERNS FOR B_n AND Q_n POINTS

In Figs. 9–20, the typical time evolution of wave-function modulus $|\psi|$ from our simulations can be seen with (a) Gaussian and (b) plane-wave initial conditions. For each n we have chosen $\tilde{v}_0 = 10^{n-3}$ and the value $v_0 = 0.2$ or $v_0 = 50$, which corresponds to B_n and Q_n points as specified in Fig. 2. In the respective captions we quote the values of v_0 and $\tau = \sqrt{\tilde{v}_0/v_0}$. The ensemble-averaged time evolution of the scintillation index $S(t)$ was laid over the plane wave simulations.

[1] M. A. Topinka, B. J. LeRoy, R. M. Westervelt, S. E. J. Shaw, R. Fleischmann, E. J. Heller, K. D. Maranowski, and A. C. Gossard, Nature (London) **410**, 183 (2001).

[2] L. Kaplan, Phys. Rev. Lett. **89**, 184103 (2002).

[3] J. J. Metzger, R. Fleischmann, and T. Geisel, Phys. Rev. Lett. **105**, 020601 (2010).

[4] M. V. Berry, Proc. R. Soc. A **463**, 3055 (2007).

[5] H. Degueldre, J. J. Metzger, T. Geisel, and R. Fleischmann, Nat. Phys. **12**, 259 (2016).

[6] H. Degueldre, J. J. Metzger, E. Schultheis, and R. Fleischmann, Phys. Rev. Lett. **118**, 024301 (2017).

[7] M. V. Berry, J. Opt. **22**, 115608 (2020).

[8] A. Patsyk, U. Sivan, M. Segev, and M. A. Bandres, Nature (London) **583**, 60 (2020).

[9] Problem No. 9 for the 34th IYPT 2021, available online on https://www.iypt.org/wp-content/uploads/2020/07/problems2021_signed-1.pdf, February 22, 2022.

[10] E. J. Heller, R. Fleischmann, and T. Kramer, Phys. Today **74**(12), 44 (2021).

[11] P. Markoš, Acta Physica Slovaca **56**, 561 (2006).

[12] S. E. J. Shaw, Propagation in smooth random potentials, Ph.D. thesis, Harvard University, 2002.